ISSN 2411-3336; e-ISSN 2541-9404

JOURNAL OF MINING INSTITUTE

Zapiski Gornogo instituta

Journal homepage: pmi.spmi.ru

Research article *Geology*

Mineralogy and thermobarometry of the Kalevian volcano-plutonic complex of the Kaskama block (Inari Terrane, Kola-Norwegian Region, Fennoscandian Shield)

Aleksandr B. Vrevsky[1,2]✉, **Anastasiya V. Yurchenko**[1], **Shauket K. Baltybaev**[1,3]

[1] *Institute of Precambrian Geology and Geochronology RAS, Saint Petersburg, Russia*

[2] *Geological Institute, Kola Science Centre of the RAS, Apatity, Russia*

[3] *Institute of Earth Sciences, Saint Petersburg State University, Saint Petersburg, Russia*

***How to cite this article*:** Vrevsky A.B., Yurchenko A.V., Baltybaev Sh.K. Mineralogy and thermobarometry of the Kalevian volcano-plutonic complex of the Kaskama block (Inari Terrane, Kola-Norwegian Region, Fennoscandian Shield). Journal of Mining Institute. 2025. N 16472, p. 1-14.

Abstract

The petrogenesis and evolution of metamorphic rocks of the volcano-plutonic units of the Kaskama block of the Inari Terrane in northwestern Russia were studied. A petrographic and mineral study and modeling of igneous and metamorphic mineral formation were performed. *PT*-conditions of rocks, along with previously known data, including geochronological ones, do not allow us to correlate the studied units with rocks of the Belomorian complex, as previously thought. Modeling of igneous and metamorphic mineral shows good convergence with the fields of stability of mineral parageneses and quantitive ratio of minerals with those observed in the real samples. The early mineral parageneses of the magmatic stage corresponds to the crystallization of rock-forming and accessory minerals from the komatiite melt, and mineral parageneses of progressive and regressive metamorphism stages are superimposed on them. Relic igneous minerals (olivine, clinopyroxene, orthopyroxene, magnetite-spinel) in metaperidotites make it possible to estimate their liquidus temperatures in the range of 1,480-950 °C. The progressive stage of metamorphism is characterized by the development of mineral parageneses: garnet + amphibole + plagioclase + quartz ± biotite, amphibole + plagioclase + quartz. The late low-temperature regressive stage of metamorphism is characterized by the development of epidote-, zoisite-, actinolite-containing associations and a number of other low-temperature minerals. Peak parameters of progressive metamorphism are estimated as T = 600-700 °C, P = 5-9 kbar and for the regressive stage as T = 400-500 °C, P = 3-5 kbar. The identified thermodynamic conditions for the Kaskama block should be considered when determining whether the studied volcano-plutonic and metasedimentary units belong to the Paleoproterozoic terranes of the Kola-Norwegian Region of the Fennoscandian Shield.

Keywords

Fennoscandian Shield; Inari Terrane; Kaskama block; metavolcanics; metaperidotites; metamorphism; *PT*-conditions

Funding

The research was carried out at the expence of a grant from the Russian Science Foundation N 24-27-00041.

Received: 02.05.2024 ***Accepted: 07.11.2024*** ***Online: 29.04.2025***

Introduction

The geological and tectonic structure of the Fennoscandian Shield in general and the Kola-Norwegian Region in particular is interpreted on the concepts of the block structure of the Earth's crust, based on fundamental differences in the tectonic development of upper crustal structures, the periodization of their endogenous evolution and the geophysical features of the deep lithosphere structure [1]. In recent decades, these concepts have been transformed into a "terrane" geodynamic paradigm. Terrane analysis has brought genetic meaning to the descriptive principles of tectonic zoning and ranking of Precambrian complexes (e.g., accretionary, dispersion, and composite terranes), which largely depends on the conceptual preferences of the

authors (plate or plume tectonic). These ideas have evolved significantly due to the emergence of new isotopic data on the age of the upper crustal geological complexes and their deep protoliths.

For the Kola-Norwegian Region of the Fennoscandian Shield (Central Kola Terrane) (Fig.1, *a*) there are several views of geodynamic models of the lithosphere development in the Early Precambrian [2-4], which have a number of fundamental differences, mainly in the interpretation of the geodynamic nature of certain terranes. One of the key regions for the reconstruction of the orogenic development of the continental lithosphere of the Kola-Norwegian Region in the Early Precambrian is the Inari Terrane [5]. The largest and least studied part of the terrane is located between the Paleoproterozoic structures of the Pasvik-Polmak-Pechenga intracraton paleorift and the Lapland Granulite Belt and extends in the southeasterly direction over more than 300 km from the Caledonides to the territory of Northern Norway and Finland.

On the territory of Russia, the Inari Terrane, which spatially corresponds to the previously identified Kaskama block (block-anticlinorium) [2, 6], borders on the Lotta-Salnotundra block of the Lapland Granulite Belt in the southwest, and in the northeast its boundary runs along the volcanogenic-sedimentary complexes of the South Pechenga zone. The Inari Terrane spatially coincides in many respects with the Pechenga-Allarechka ore region [7], which determines the relevance of its study in the metallogenic aspect.

There are only general ideas about the structure of the Inari Terrane as a tectonic mixture (tectonic packages) of the Archean and Proterozoic complexes [3, 4, 8], and within the framework of theoretical geodynamic constructions this area is considered as part of the Inari-Tersk juvenile arc, which arose as a result of a two-stage collision with the subsequent formation of a secondary orocline [4, 8]. Such a diversity of geodynamic ideas is largely determined by the limited amount of modern petrological-geochemical and isotopic data [9-11].

In different years, in the northwest of the Kola Peninsula, within the limits corresponding to the modern concepts of the tectonic boundaries of the Inari Terrane, in large synclinal structures researchers identified the essentially volcanogenic Kaskama Formation of uncertain Neoarchean-Paleoproterozoic age. Nowadays, due to the obtained U-Pb isotope age (1,923-1,926 Ma) of acidic and middle metavolcanic rocks, the Kaskama Formation was assigned to the Kalevian suprahorizon of the Karelian complex [5, 6], which fundamentally changes the ideas about the geological structure and metallogenic zonation of the Pechenga-Allarechka ore region and the geodynamic nature of the Inari Terrane.

The goal of the work is to determine the conditions of petrogenesis of mantle magmatism and thermobaric evolution of the regional metamorphism of the volcano-plutonic complex of the Kaskam structure based on solving the problems of detailed petrography, analyzing the features of the chemical composition of minerals and determining the *PT*-parameters of metamorphic changes. The study is directed at obtaining new knowledge about the correlation of endogenous processes and comparing the geological structure and tectonic evolution of the adjacent blocks of the Kola-Norwegian Region, which is the most important tool for terrane analysis of the Fennoscandian Shield.

Methods

The study of the structure of minerals and analysis of their compositions were performed on a scanning electron microscope JSM-6510LA with EDS JEOL JED-2200 (IGGD RAS, analyst O.L.Galankina) at an accelerating voltage of 20 kV, current of 1 nA, with ZAF-method of correction of matrix effects. The detection limit of elements is 0.1 %. Photographs of minerals were obtained in the modes of compositional contrast (BSE) and secondary electron imaging (SEI).

Mineral geothermometers. We used for Ol-Cpx thermometry equation [12], based on Fe-Mg exchange between augite and olivine; for Cpx-Ol-Spl thermometry – the equation developed for spinel peridotites [13]; for Ol-Spl thermometry – the equilibrium equation by [14]; for the paragenesis of two pyroxenes geothermometers [15, 16]; for the paragenesis of amphibole with plagioclase – the geothermometer by T.Holland and R.Blandy [17]; for the paragenesis of garnet and amphibole – several thermometric tools, calibrations of which are given in [18-21]; for the paragenesis of garnet and biotite – a thermometer [22].

Mineral geobarometers – monomineral amphibole [23], garnet-amphibole-plagioclase [24-26], garnet-biotite-plagioclase for quartz-bearing rocks [27].

Calculation of stability fields of mineral paragenesis was performed using the Perple_X v.6.9.1 [28] with updates up to 2022. In calculations we used the thermodynamic database hp62ver [29] for minerals and solid solutions of clinoamphibole cAmph(G), orthoamphibole oAmph(DP), clinopyroxene Omph(GHP), olivine O(HP), talc T, biotite Bio(TCC), feldspars, chlorite Chl(W), garnet Gt(W), spinel Sp(WPC), orthopyroxene Opx(W), white mica Mica(CHA), chloritoid Ctd(W), staurolite St(W), ilmenite Ilm(WPH) in the MnTiNCKFMASH-CO_2 system (MnO-TiO_2-Na_2O-CaO-K_2O-FeO-MgO-Al_2O_3-SiO_2-H_2O), as well as the model of silicate melt(G) [30, 31].

The order of crystallization of minerals was determined in a rock of peridotite composition together with an estimate of liquidus temperatures for olivine, pyroxenes, plagioclase and magnetite were determined together with the estimations according to the equations of mineral-melt system based on COMAGMAT 3.73 software package [32].

Representative chemical analyses of the main rock varieties of the Kaskama Formation (Table 1) and about 400 microprobe analyses of minerals were used to model mineral formation and estimate *PT*-parameters. Abbreviations of mineral names are given according to [33], and calculation of mineral formulas according to [34].

The geological structure of the region and composition of rocks

In the northwestern part of the Kola Peninsula, the most preserved and accessible fragment of the Kaskama Formation supracrustal complex are two associated synclinal structures over 25 km long in the Kuroaivi, Korablekk, Kaskama, Shuort tundra, 40 km southwest of the Pechenga structure (Fig.1, *a*).

The lower part of the section of the volcano-sedimentary complex of the Kaskama Formation (over 3,000 m) is represented mainly by various amphibolites and Grt-Bt-Amp schists, which corresponds to tholeiitic and aluminous metabasalts (Table 1). A characteristic feature of the crossection is the presence of metaultramafic bodies, amphibolites, and actinolite-chlorite schists, 15-20 m thick and more than 300 m long, the chemical composition of which corresponds to komatiites and komatiite basalts (Table 1). The structural and geological position of these rocks allows us to consider some of them as metamorphosed volcanic flows, sills and hypabyssal intrusions, and the largest massifs are probably pre-folded intrusions of peridotites. The overlying middle stratum of garnet-biotite-amphibole gneisses and plagioschists with amphibolite interlayers composes two synclinal structures (Fig.1, *b*). In the upper part of the middle strata there are several units of fine-grained plagioschists, leucocratic biotite-feldspar gneisses and amphibolites with a thickness of 20-30 m, which are considered as metamorphosed analogues of felsic and intermediate volcanics and their tuffs (Table 1).

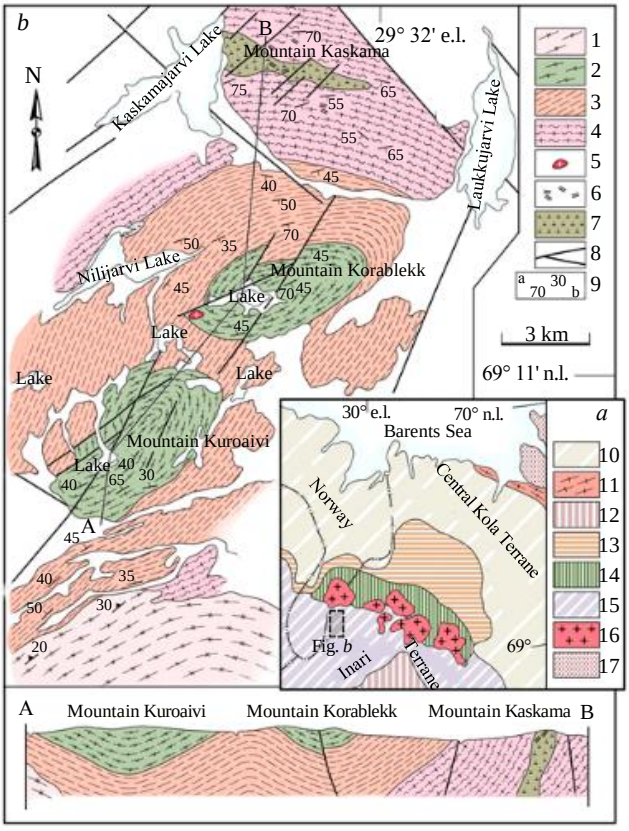

Fig.1. A geological scheme of the Kaskama structure [35] with corrections

1 – tonalite gneisses; 2-4 – supracrustal complex of the Kaskama Formation (2 – upper, 3 – middle and 4 – lower strata); 5 – plagiomicrocline granites; 6 – metagabbro; 7 – metaultramafic dikes; 8 – faults; 9 – structural elements (a – layering, b – gneissic banding); 10 – Central Kola Terrane; 11 – Murmansk Terrane; 12 – Lapland Granulite Belt; 13 – North Pechenga zone; 14 – South Pechenga zone; 15 – Inari Terrane; 16 – tonalite and plagiogranite intrusions; 17 – Vendian deposits

Table 1

Content of petrogenic oxides in the main types of rocks of the Kaskama Formation, wt.%

Petrogenic oxides	Samples								
	1	2	3	4	5	6	7	8	9
	104	20-3d	106	18-5b	101-1	17-3a	8-12	8-6	17-4a
SiO_2	42.00	42.60	39.60	40.00	47.15	46.20	52.75	78.95	71.00
TiO_2	0.13	0.10	0.09	0.07	0.53	0.44	0.48	0.19	0.20
Al_2O_3	8.30	10.45	13.75	13.50	19.60	20.00	16.55	9.90	12.80
Fe_2O_3	5.52	3.79	3.97	2.83	1.85	3.35	2.41	1.22	0.90
FeO	8.54	8.41	8.67	9.32	9.96	9.32	7.63	3.10	4.92
MnO	0.20	0.18	0.19	0.15	0.23	0.18	0.20	0.10	0.10
MgO	21.95	20.00	20.00	20.00	6.50	5.48	4.91	0.32	1.51
CaO	7.69	10.21	12.24	7.52	11.20	12.08	9.88	2.74	5.05
Na_2O	0.27	0.32	0.37	0.44	1.41	1.18	2.51	2.67	2.72
K_2O	0.07	0.28	0.04	0.18	0.14	0.09	0.53	0.45	0.15
P_2O_5	0.07	0.03	0.03	0.03	0.05	0.03	0.19	0.06	0.10
LOI	5.84	3.92	3.30	6.30	1.62	1.99	1.66	0.34	0.93
Total	100.58	100.29	100.25	100.34	100.24	100.34	99.70	100.04	100.38
CaO/Al_2O_3	0.9	1.0	0.9	0.8	–	–	–	–	–
Al_2O_3/TiO_2	64	86	153	193	51	–	–	–	–
CIA	–	–	–	–	–	–	51	49	48
al'	0.23	0.32	0.42	0.42	1.1	1.1	–	–	–

Notes.
al' = $Al_2O_3/(MgO + Fe_2O_3 + FeO)$ – alumina content index, wt.%.
CIA = $100 \times [Al_2O_3/(Al_2O_2 + CaO + Na_2O + K_2O)]$ – chemical index of alteration, mol.%.
1-4 – metaperidotites; 5, 6 – garnet-amphibole schist and garnet-epidote-containing amphibolite (aluminous metabasalts); 7 – epidote-containing amphibolite (metaandesite); 8, 9 – amphibole-plagioclase schist and migmatized garnet-amphibole-plagioclase schist (acid metavolcanics).

The core parts of the synclines (Fig.1) are composed of the upper strata of the Kaskama Formation, represented mainly by fine- to medium-grained slate and massive amphibolites with interlayers of actinolite-chlorite schist similar in composition to komatiite basalts and tholeiitic and aluminous metabasalts of the lower strata of the section.

Petrographic and mineralogical description of rocks and features of chemical composition of minerals

Metamorphosed peridotite (samp. 104, 20-3d, 106, 18-5b). *Petrography.* Amount of the minerals in the rocks, vol.%: olivine 20-40; orthopyroxene up to 5; hornblende up to 10; clinopyroxene 20-40; plagioclase 20-30; green spinel up to 5. In massive rocks from sills and hypabyssal intrusions an early (magmatic) paragenesis consisting of olivine (later serpentinized), clinopyroxene, orthopyroxene, plagioclase, and spinel is rather clearly diagnosed. Metamorphic minerals include amphibole, epidote, chlorite, spinel, and magnetite. Olivine forms colorless isometric grains up to 1-1.5 cm in size and has a reticulate structure due to multiple cracks (Fig.2, *a*, *b*), filled with serpentine, which contains new formed magnetite. Light-green tremolite develops along the edge of olivine grains, and worm-like spinel outgrowths (Fig.2, *b*), oriented perpendicular to the rim develop at the contact with plagioclase. Clinopyroxene occurs both in inclusions in olivine and as xenomorphic grains in the matrix. It is often replaced by amphibole along grain margins and along cleavage cracks. Orthopyroxene is developed in the form of single small xenomorphic grains, as a rule, at the contact with olivine in the form of a thin border between olivine and amphibole. Green spinel is located both in the matrix as large individual grains and in symplektitic concretions with amphibole. Plagioclase often has polysynthetic twinning and is preserved and recognized

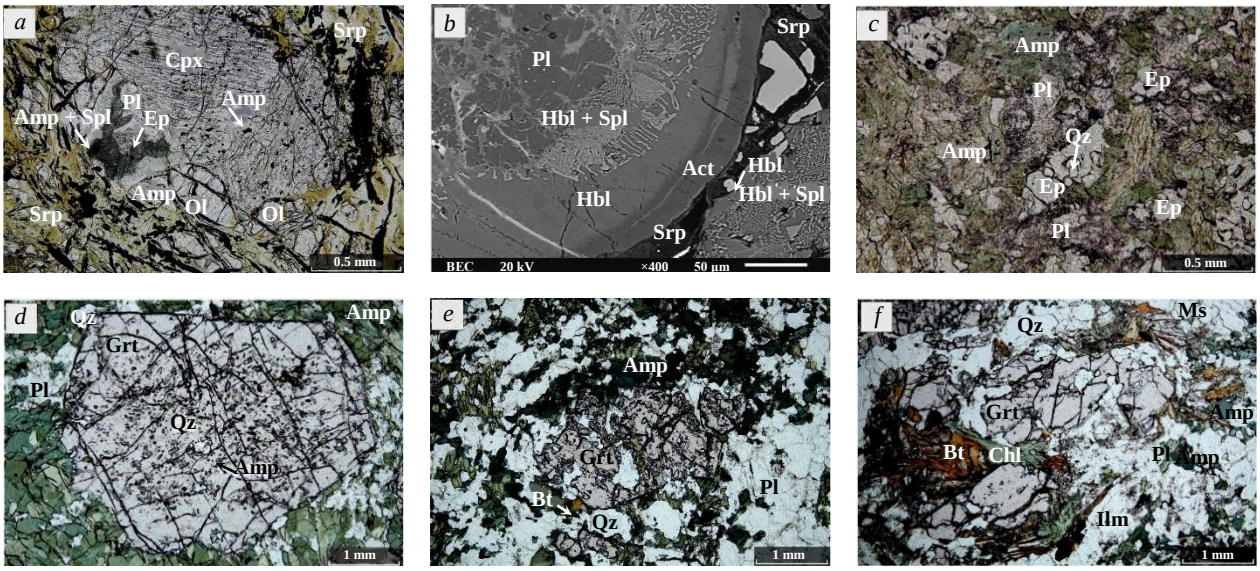

Fig.2. Microphotographs of thin sections in transmitted light (*a*, *c*-*f*) and BSE (*b*) of the Kaskama Formation rocks: *a* – metamorphosed peridotite (samp. 104), serpentinized Ol, Cpx replacing Hbl, Ep replacing Pl, Spl+Hbl symplectites after Pl; *b* – metamorphosed peridotite (samp. 104), Spl+Hbl symplectites, zonal Amp border at the contact of Ol with Pl; *c* – epidote-bearing amphibolite (samp. 8-12), epidote grains contain quartz inclusions, plagioclase is altered; *d* – garnet-amphibole schist (samp. 101-1), Grt with formed facets contains Qz and Amp inclusions, enveloped by prismatic light-green Amp; *e*, *f* – migmatized garnet-amphibole-plagioclase schist (samp. 17-4a), Grt in Pl-Amp matrix, replaced by Chl-Bt-Ms aggregate, contains Qz and Pl inclusions

within the amphibole-spinel symplectite. Clusters of epidote-zoisite units are observed in plagioclase. In some places large grains of hornblende (up to 2 mm) saturated with ilmenite inclusions are observed. Local replacement of amphibole by actinolite-tremolite assemblage together with needles of chlorite is also noted.

Mineral composition. Olivine as forsterite with X_{Mg} = Mg/(Mg + Fe) = 0.72-0.75 in large grains, in small grains has X_{Mg} = 0.66 without Cr_2O_3 impurity, in single analyses NiO content up to 0.28 wt.%, and also there is a constant addition of MnO – 0.19-0.74 wt.%. Clinopyroxene is represented by diopside with X_{Mg} = 0.86-0.94, small addition of Cr_2O_3 up to 0.41 wt.%, TiO_2 up to 0.31 wt.% and MnO up to 0.22 wt.% in separate grains, Al_2O_3 content – 0.54-2.8 wt.%. The highest aluminum content is detected in clinopyroxene, which forms inclusions in olivine. Orthopyroxene corresponds to enstatite with X_{Mg} = 0.74-0.79, and contains addition of MnO (0.33-0.72 wt.%) and Al_2O_3 (0.51-1.65 wt.%). Plagioclase mostly is anorthitic in composition (An = 94-100 %).

Spinel corresponds to $Hc_{43-54}Spl_{44-54}Mg_{2-4}$, contains a small admixture of zinc (ZnO = 0.11-0.49 wt.%), manganese (MnO = 0.26-0.9 wt.%). No obvious differences in the composition of large spinel grains and its sprouting in the form of symplectites were revealed.

Amphibole is mainly represented by magnesio-hornblende (Fig.3, *a*) with X_{Mg} = 0.79-0.89. In symplectite with spinel, amphibole is more rich Al_2O_3: it corresponds to chermakite with Al_2O_3 = 14.2-17.5 wt.%, and in the rim – to hornblende with Al_2O_3 = 5.5-13.4 wt.%. The symplectite also contains larger portions of hornblende, with composition corresponding to those in the rims. The hornblende, developing upon clinopyroxene, contains a highly addition of TiO_2 = 0.1-0.75 wt.%.

Aluminous metabasalt (epidote-bearing amphibolite, samp. 8-12). *Petrography.* Amount of minerals, vol.%: epidote up to 10; plagioclase up to 20; amphibole up to 55; quartz up to 15; chlorite up to 5; accessory apatite, titanite, and magnetite. The rock texture is mainly poikiloblastic, granonematoblastic, and the structure is massive. In the epidote-amphibole matrix there is no noticeable preferential orientation of minerals (Fig.2, *c*). Epidote up to 0.5 mm, contains rounded inclusions of quartz, allanite. Plagioclase is altered, grain size up to 0.3 mm, replaced by zoisite. Amphibole is light-green,

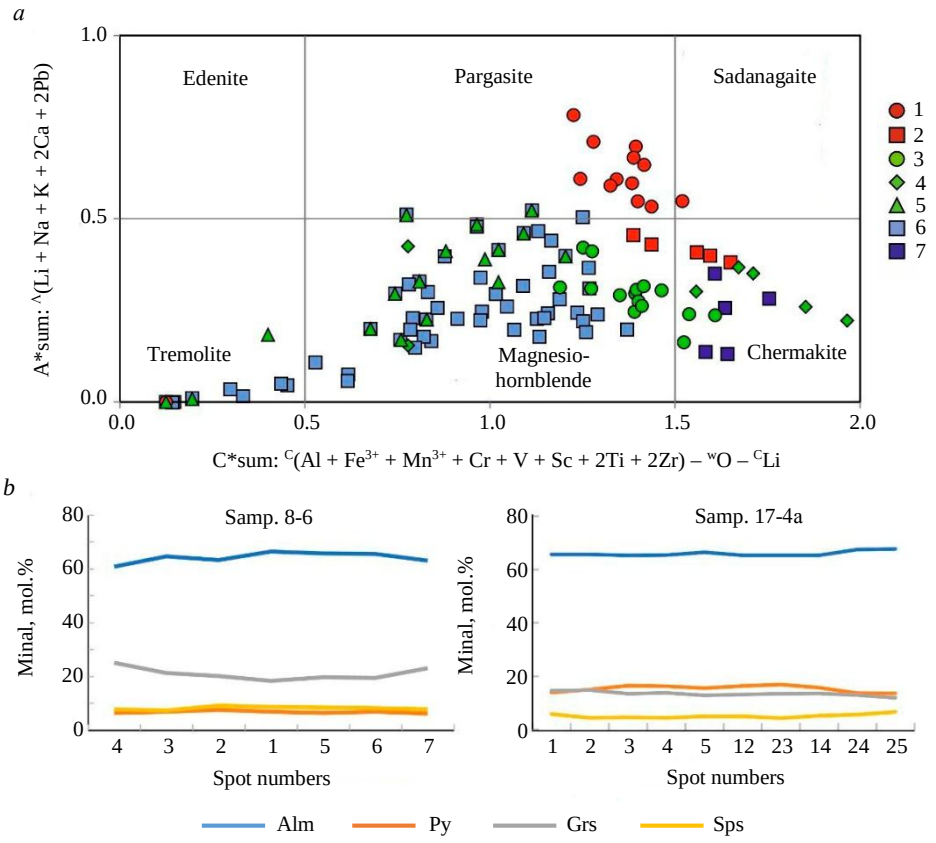

Fig.3. Features of mineral composition of rocks of the Kaskama Formation:
a – chemical composition of amphibole by [36], the coordinates of the axes correspond to the sum of the cation contents in the mineral, in felsic metavolcanite (1 – samp. 8-6; 2 – samp. 17-4a), aluminous metabasalt (3 – samp. 101-1; 4 – samp. 17-3a), metaandesite (5 – samp. 8-12), metaperidotite (6 – samp. 104; 7 – from the same sample, but amphibole as part of symplektitic intergrowths);
b – chemical profiles across of garnet grain from amphibole-plagioclase schist (samp. 8-6) and migmatized garnet-amphibole-plagioclase schist (samp. 17-4a)

browner along the cleavage cracks, replaced by chlorite. Quartz is rounded grains up to 0.1 mm in close association with epidote, it is also found in small amount in inclusions in amphibole. In lightened areas of the rock, epidote with quartz inclusions has grain size up to 0.5 mm, plagioclase is more altered, and quartz grains become larger – up to 0.4 mm.

Mineral composition. Plagioclase in amphibolite is andesine (An = 44-53 %), but in case of replacement by epidote it is close to pure albite (An = 2-16 %). Amphibole is represented by pargasite and magnesio-hornblende (Fig.3, *a*), in association with chlorite early amphibole is replaced by actinolite. In the more leucocratic part of the rock, the magnesio-hornblende is a little more ferrous with X_{Mg} = 0.53-0.65, contains more TiO_2 (0.37-0.85 wt.%), Na_2O (0.76-1.55 wt.%) и Al_2O_3 (7.92-14.0 wt.%), less Cl (0.11-0.28 wt.%) than magnesio-hornblende with X_{Mg} = 0.61-0.70 in amphibolite, contains TiO_2 (0.40-0.81 wt.%), Na_2O (0.6-1.6 wt.%), Al_2O_3 (7.4-11.4 wt.%), Cl (0.15-0.19 wt.%). The later actinolite has a X_{Mg} = 0.71-0.72 and contains TiO_2 (0-0.61 wt.%), Na_2O (0-0.23 wt.%), Al_2O_3 (0.75-5.41 wt.%), Cl (0-0.08 wt.%).

Aluminous metabasalt (garnet-epidote-bearing amphibolite, samp. 17-3a). *Petrography.* Mineral composition, vol.%: amphibole up to 65; plagioclase up to 15; epidote up to 10; quartz 10; single grains of garnet; secondary minerals – chlorite, accessory ilmenite. It is a coarse-grained heterogeneous rock in which the amphibole-plagioclase matrix contains porphyroblasts of amphibole up to 4 mm in size and single garnet grains up to 2 cm in size (Fig.2, *d*). Amphibole grains with abundant inclusions of ilmenite needles and rounded quartz grains up to 0.1 mm in size, as well as smaller amphibole grains without inclusions, occur. Garnet porphyroblasts sometimes contain inclusions of large (up to 1 mm) grains of epidote-zoisite and ilmenite, as well as quartz, plagio-

clase, and amphibole in the core; the rims do not contain inclusions. Leucocratic parts of the rock are represented by quartz-epidote-plagioclase aggregates. Plagioclase grains up to 1 mm in size with polysynthetic twins are placed between amphibole grains. Epidote and zoisite develop on plagioclase. Chlorite develops in separate grains on amphibole.

Mineral composition. Garnet is grossular-almandine $Py_{9-14}Alm_{65-72}Sps_{2-5}Grs_{15-19}$. There is a tendency for the grossular and pyrope to increase towards the rim with a decrease in almandine. Amphibole next to garnet is represented by magnesio-hornblende with X_{Mg} = 0.55-0.56, contains TiO_2 (0.68-0.77 wt.%), Na_2O (0.68-0.82 wt.%), Al_2O_3 (7.16-7.50 wt.%), cummingtonite with X_{Mg} = 0.44 at the contact with garnet and at the rim of hornblende; in the garnet-free matrix amphibole is represented by ferri-chermakite with c X_{Mg} = 0.39-0.44 and contains TiO_2 (0.14-0.35 wt.%), Na_2O (1.17-1.62 wt.%), Al_2O_3 (17.3-20.1 wt.%). Plagioclase is heterogeneous, characterized by more felsic inclusions (An = 52-68 %, labrador) in more basic grains (An = 87-92 %, bytownite-anorthite), at the contact with garnet plagioclase has the composition of labrador (An = 54-64 %). Chlorite in the form of large grains ~3 мм mm at the contact with amphibole has X_{Mg} = 0.57-0.58.

Aluminous metabasalt (garnet-amphibole shale, samp. 101-1). *Petrography.* Amount of minerals, vol.%: garnet up to 15; amphibole 50; plagioclase up to 25; quartz up to 10. In the plagioclase-amphibole matrix of the rock there are porphyroblasts of garnet with well-formed grain up to 1.5 cm in size. These porphyroblasts contain many inclusions of quartz, plagioclase, and amphibole in the core of the grains, the rims of the grains are without inclusions. Plagioclase, with grain size up to 0.5 mm, together with amphibole up to 0.6 mm, is arranged parallel to layering, thus surrounding the garnet porphyroblasts (see Fig.2, *d*).

Mineral composition. Garnet is pyrope-almandine $Py_{22-26}Alm_{58-63}Sps_{3-4}Grs_{11-16}$ with minor zoning, showing a decrease of pyrope with an increase of the grossular and almandine toward the grain rim. In the matrix, plagioclase is a composition of bytownite (An = 78-82 %), to the contact with garnet and amphibole some grains have a slight zoning – the content of anorthitic component decreases up to An = 48-58 %. In the garnet inclusions, the plagioclase composition is more basic (An = 86-87 %) than in the matrix. Amphibole is a composition of magnesio-hornblende (Fig.3, *a*), at the contact with garnet it is closer to chermakite with X_{Mg} = 0.57-0.66, contains TiO_2 = 0.41-0.83 wt.%, Na_2O = 1.04-1.67 wt.%, Al_2O_3 = 14.2-15.11 wt.%.

Metarhyolite (amphibole-plagioclase schist, samp. 8-6). *Petrography.* Amount of minerals, vol.%: amphibole up to 20; plagioclase up to 30; quartz up to 50; single grains of biotite, chlorite, and garnet, accessory ilmenite, apatite, zircon. The rock consists of green, light-green amphibole with grain size up to 2 mm, elongated parallel to layering. Inclusions of accessory minerals and quartz occur in the amphibole. The texture is heterogeneous: in the more leucocratic part there is an enlargement of amphibole grains up to 3 mm, while their number becomes noticeably smaller. In the most leucocratic parts of the rock there are only single grains of amphibole between quartz grains. Amphibole is partially chloritized. Biotite occurs in the form of thin grains. Closer to the garnet, biotite becomes noticeably more abundant, where it is intergrown with amphibole, and in some places, it develops on altered plagioclase. Plagioclase often with twins, grain size up to 3 mm, with their size increasing in the leucocratic part up to 5 mm, it is subjected to replacement by carbonate-mica aggregate (not more than 10 vol.%). In the leucocratic part, plagioclase grains, as well as quartz ones, are elongated along the direction of layering and often with corroded rims. Sometimes plagioclase contains quartz and amphibole inclusions. Single garnet grains occur in both melanocratic and leucocratic parts. The size of garnet in the melanocratic part of the rock is larger (up to 2 mm) than in the leucocratic (up to 1 mm). In the leucocratic part, garnet is replaced by chlorite in association with ore (ilmenite) and later plagioclase (albite).

Mineral composition. The composition of amphibole in the leucocratic part is more ferrous with X_{Mg} = 0.25-0.32, in addition to ferro-pargasite there is also hastingsite (see Fig.3, *a*). The content of TiO_2 = 0.59-1.14 wt.%, Al_2O_3 = 13.5-14.7 wt.%, Na_2O = 1.42-1.89 wt.%, Cl = 0.33-0.48 wt.%. In the melanocratic part of the rock amphibole is represented by ferro-pargasite with X_{Mg} = 0.29-0.32, contains TiO_2 = 0.46-1.16 wt.%, Al_2O_3 = 13.7-15.1 wt.%, Na_2O = 1.3-1.86 wt.%, Cl = 0.25-0.40 wt.%. Biotite of the investigated sample belongs to ferrous varieties (X_{Mg} = 0.35) with

predominance siderophyllite and contains TiO_2 (3.3-3.4 wt.%). The composition of plagioclase within the sample is homogeneous (An = 26-29 %) and corresponds to oligoclase, except for its rims around garnet, where its composition is more felsic (An = 8-10 %). Grossular-almandine garnet $Py_{6-7}Alm_{61-66}Sps_{7-9}Grs_{18-25}$ in the leucocratic part and $Py_{7-8}Alm_{62-65}Sps_{8-9}Grs_{19-23}$ in the melanocratic part, are in association with amphibole. These garnets are equally characterized by a decrease in almandine and spessartine and an increase in grossular from core to rim (Fig.3, *b*).

Metarhyodacite (migmatized garnet-amphibole-plagioclase schist, samp. 17-4a). *Petrography.* Amount of minerals, vol.%: garnet up to 5; amphibole up to 20; plagioclase up to 30; quartz up to 45; single grains of biotite, muscovite and chlorite, accessory ilmenite. The rock is heterogeneous and represents migmatized garnet-bearing amphibolite. Garnet porphyroblasts up to 1 cm in size at the contact with the leucocratic part (see Fig.2, *e*, *f*) with abundant quartz and plagioclase inclusions. The sample under consideration differs from the previous sample by larger grain sizes, absence of preferred orientation of minerals, greater development of chlorite both in association with amphibole and developing on garnet. Together with chlorite there are biotite and muscovite, which in some places develop on plagioclase. Accessory minerals are represented by ilmenite with inclusions of rutile, which in turn develops titanite.

Mineral composition. Garnet is grossular-pyrope-almandine $Py_{11-18}Alm_{65-71}Sps_{4-9}Grs_{9-15}$. It is characterized by an increase almandine and spessartine and a decrease pyrope and grossular from core to rim (Fig.3, *b*). The most ferrous composition has garnet replaced by chlorite, $Py_{11-13}Alm_{70-71}Sps_{7-9}Grs_{10}$. Plagioclase has oligoclase (An = 28-31 %), the greatest changes are observed in plagioclase in the leucocratic part of the rock, where plagioclase becomes slightly more anorthitic (An = 33 %). Amphibole in the rock is represented by magnesio-hornblende and chermakite (Fig.3, *a*) with X_{Mg} = 0.42-0.46, contains TiO_2 (0.20-0.44 wt.%), Na_2O (1.54-1.66 wt.%), Al_2O_3 (16.6-17.55 wt.%). Chlorite is more ferrous at the contact with garnet, possibly developing over amphibole, X_{Mg} = 0.43-0.47. Chlorite developing on small garnet grains and plagioclase has X_{Mg} = 0.31-0.39.

Magmatic stage of crystallization

To determine the *PT*-conditions of crystallization of magmatic minerals the compositions of metamorphosed peridotites were used – samples 104, 106, 18-5b, 20-3d (Tables 1, 2), in which the structural and textural features and minerals of the magmatic stage of rock formation were well preserved.

Table 2

Liquidus temperatures of mineral crystallization of the rocks of peridotite composition of the Kaskama Formation, °C

Sample	Ol-melt	Opx-melt	Aug-melt	Mt-melt	Pl-melt
106	1,478	–	1,285	1,187	1,074
20-3d	1,457	–	1,307	1,184	1,036
18-5b	1,486	1,168	1,284	1,189	1,073
104	1,493	1,172	1,312	1,199	955

Notes. Liquidus temperatures are calculated using the mineral-melt equations from the COMAGMAT 3.73 [32].

The identified primary mineral paragenesis consisting of olivine, two pyroxenes, plagioclase with some amount of magnetite-spinel is well reproduced by model of equilibrium crystallization in COMAGMAT program (Fig.4). In this case, in addition to the coincidence of the composition of minerals during their formation from the melt, the volume ratios established by petrographic data are also reproduced. In addition to reproducing the order of mineral crystallization and their amount, the results of modeling showed a good correspondence between the calculated compositions of minerals (olivine, pyroxenes, and plagioclase) and those actually observed in the rocks. In particular, magnesium number in olivine decreases from ~ 0.94 to 0.70, and plagioclase changes from almost pure anorthite to bytownite, demonstrating a decrease in the number of plagioclases with decreasing of crystallization temperature (Fig.4, *a*).

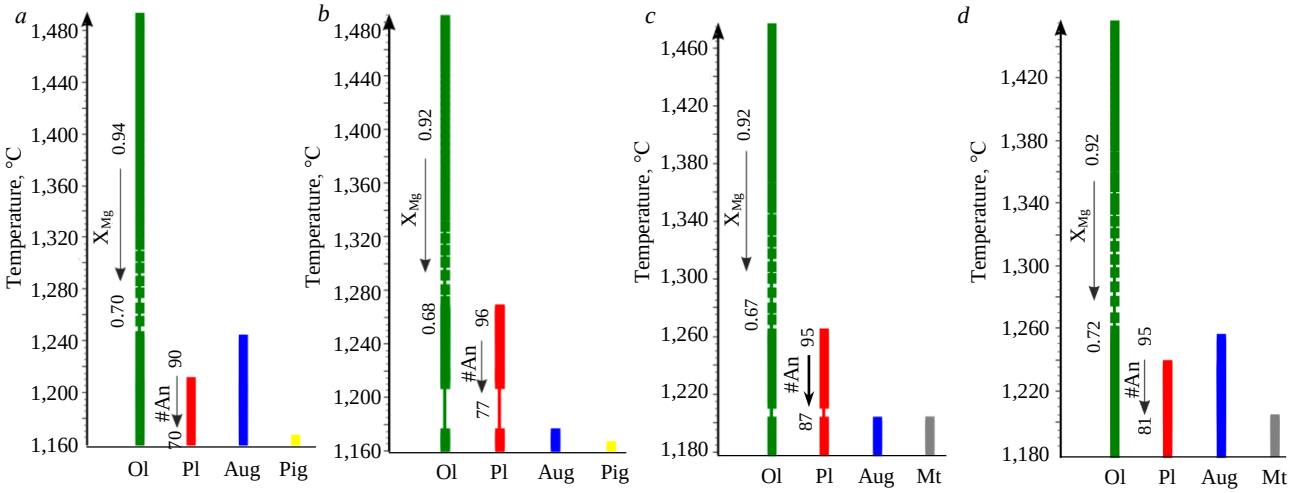

Fig.4. Sequence of equilibrium magmatic crystallization of minerals from melt according to the COMAGMAT program for samples of metamorphosed peridotite: *a* – samp. 104; *b* – samp. 18-5b; *c* – samp. 106; *d* – samp. 20-3d. The compositions of olivine and plagioclase are consistent with the real compositions of minerals according to microprobe analysis data

Additionally, the temperatures and crystallization sequence of minerals obtained using the equilibrium equations in the mineral-melt system were calculated (Table 2). The temperature calculation equations of the COMAGMAT software package showed that the liquidus temperatures for olivine and pyroxenes are in the range of ~1,500-1,200 °C. For plagioclase, the equilibrium temperature in the plagioclase-melt system is determined as 955 °C, but the first crystallization of the mineral begins at T = 1,202 °C.

PT-conditions of metamorphism

To assess the thermodynamic stability regimes of mineral parageneses with changing P and T for the studied main types of rocks (see Table 1), the method of constructing pseudo-sections was used. In addition to assessing the stability of mineral parageneses with changing pressure and temperature regimes, variations in the CO_2 and H_2O ratio in the assumed dioxide-water fluid were evaluated. The calculations showed that the most relevant (corresponding to the observed) results are obtained using pure aqueous fluid without CO_2 admixture. Using the Perple_X [28], phase diagrams were constructed for rocks corresponding to the composition of the initial protolith (Fig.5). The diagrams reproduce well the association of metamorphic minerals observed in thin sections.

The widespread metamorphic mineral paragenesis in the rocks, consisting of garnet, amphibole, plagioclase, and secondary clinopyroxene, is modeled in the area of average values of pressure and temperature – T ~700 °C; P ~5-7 kbar. The range of P and T corresponds to the superposition of isopleths of these minerals, close to the real compositions of minerals according to microprobe analysis data.

The migmatization observed in some rocks (for example, in garnet-amphibole-plagioclase schist, samp. 17-4a) allows us to narrow down considerably the possible *PT*-field of metamorphic mineral formation. Thus, considering the appearance of anatectic melt in the studied rock, the *PT*-filed of metamorphic is estimated as T = 710-760 °C and P = 6-8 kbar (Fig.5, *b*).

The results of classical mineral thermobarometry do not contradict the estimates of P and T mineral formation obtained by the pseudo-section method. For rocks that have preserved magmatic and metamorphic mineral paragenesis (e.g., sample 104), pressures and temperatures corresponding to the magmatic stage of mineral crystallization and the subsequent medium-temperature and medium-baric regime of metamorphic transformations are revealed (Table 3). The use of mineral thermometers and barometers based on the chemical compositions of coexisting minerals to certain values of pressure and temperature allowed us to determine the high-temperature stage of mineral formation (olivine-spinel-pyroxene, pyroxene thermometers), correlated with the stage of magmatic crystallization of minerals and melt.

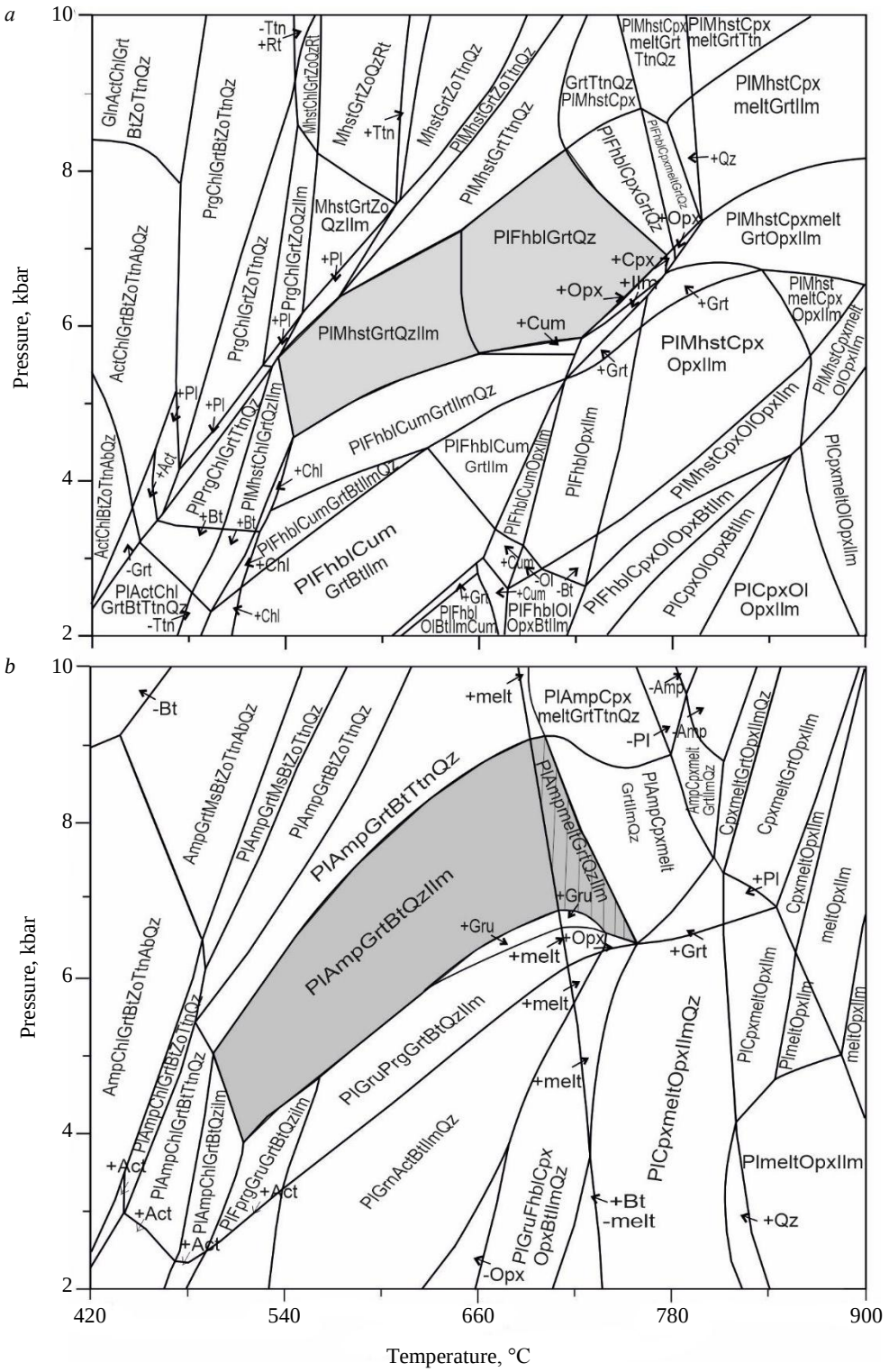

Fig.5. *PT*-diagrams of phase equilibria calculated by the method of Gibbs energy minimization in the Perple_X software: *a* – garnet-epidote-bearing amphibolite (samp. 17-3a); *b* – migmatized garnet-amphibole-plagioclase schist (samp. 17-4a). The areas corresponding to the observed garnet-bearing mineral parageneses in the studied rocks are highlighted in gray. The shading shows the *PT*-range of formation of the observed metamorphic mineral parageneses of the considered schist in the conditions of partial melting of the rock

The predominant majority of mineral geothermometers using the compositions of amphiboles, biotites, plagioclases, and garnets indicate a metamorphic temperature of rocks in the range of ~580-700 °C at a pressure of 5-9 kbar (Fig.6).

Table 3

***PT*-parameters of the rocks of the Kaskama Formation**

Sample	CpxOl	CpxOl	GrtHbl	GrtHbl	GrtHbl	GrtHbl	HblPl	GrtBt	GrtHblPl	GrtHblPl	Hbl	GrtBtPl
	L96	MG15	GP84	P91	P85	R00	HB94	H00	DHP00	KS89	M16	WZR04
	Temperature, °C						Pressure, kbar					
104	940-1,120	1,120-1,230	–	–	–	–	–	–	–	–		
101-1	–	–	585-665	620-720	580-640	465-655	640-820	–	4.4-9.9	3.4-6.8		
8-12	–	–	–	–	–	–	590-730	–	–	–		
17-3a	–	–	–	–	–	–	647-800	–	–	–		
8-6	–	–	660	670	615	580	620	660-720	6.9-8.0	6.9-7.8		9.7-9.8
17-4a	–	–	585-645	590-675	580-620	650-670	575-700	690-700	5.9-9.4	8.3-8.6	8.3-8.4	

Notes. Geothermometers: L96 [12], MG15 [13], GP84 [18], P91 [20], P85 [19], R00 [21], HB94 [17], H00 [22]; geobarometers: DHP00 [25], KS89 [24], M16 [23], WZR04 [27].

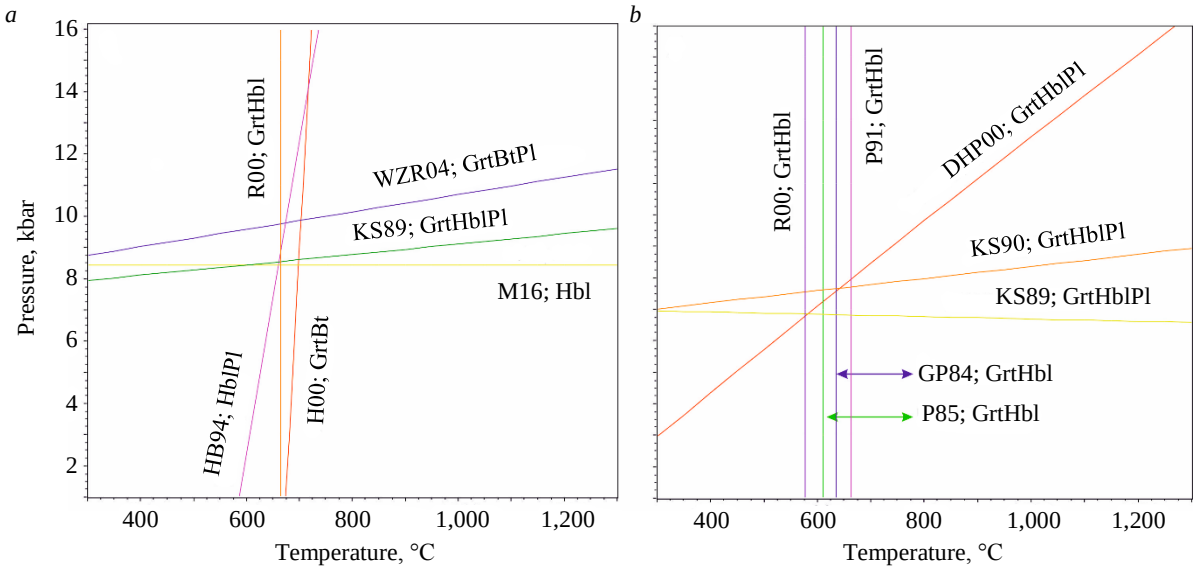

Fig.6. *PT*-diagrams with the results of calculation of metamorphism parameters of the studied schists: *a* – samp. 17-4a (migmatized garnet-amphibole-plagioclase schist); *b* – samp. 8-6 (amphibole-plagioclase schist). Calculation lines for mineral thermometers and barometers correspond to: GP84 [18], P85 [19], KS89 [24], KS90 [25], P91 [20], HB94 [17], H00 [22], DHP00 [26], R00 [21], WZR04 [27], M16 [23]

The thermobarometry results are consistent with the observed mineral parageneses in rocks of the Kaskam structure of both the magmatic and metamorphic stages. It should be noted that in recent years the success of using thermobarometric tools to assess the conditions of formation of mineral parageneses in both magmatic [37-40] and metamorphic has been repeatedly demonstrated [41-46].

It was possible to trace the evolution of thermodynamic regimes of petrogenesis in different tectonic settings, for example, subduction zones [47-49] or under extreme temperature conditions [44].

Many works are devoted to the reconstruction of *PT*-parameters of metamorphism based on the use of geochemical features of minerals [50-52] or on numerical model reconstructions of mineral formation [53-55]. This approach has shown promise for rocks of different compositions and contrasting geodynamic settings of the occurrence [56-58].

Conclusion

Modeling with Gibbs energy minimization of magmatic and metamorphic mineral formation in the rocks of the Kaskama Formation showed good convergence the stability of mineral paragenesis and quantitative ratio of minerals with those observed in real samples. Estimates of *PT*-parameters of metamorphic mineral formation using a set of modern mineral thermometers and barometers,

which consider compositions of a larger number of coexisting minerals, satisfactorily reveals the stability fields of mineral paragenesis. It allows us to distinguish two stages of mineral formation. The first magmatic stage corresponds to crystallization of olivine, clinopyroxene, orthopyroxene, magnetite-spinel from komatiite melt in the temperature range of 1,480-950 °C. The second stage of mineral formation corresponds to progressive metamorphism and its low-temperature regressive path. The progressive path of metamorphic changes is recorded in all groups of rocks of the Kaskama Formation and is characterized by extensive development of mineral paragenesis: garnet + amphibole + plagioclase + quartz ± biotite, amphibole + plagioclase + quartz. The late part (low-temperature regressive) of the path of metamorphism is characterized by the development of epidote-, zoisite-, and actinolite-bearing paragenesis, as well as serpentine, chlorite, and other low-temperature minerals by minerals forming the early paragenesis. The peak parameters of a regional metamorphism (T = 600-700 °C, P = 5-9 kbar) and its regressive part (T = 400-500 °C, P = 3-5 kbar) for rocks of the Kaskama block are different from the peak parameters obtained for the South Pechenga zone (T = 590-750 °C, P = 9.5-10.6 kbar [59] and T = 630-690 °C, P ~5 kbar). These results indicate that there are no signatures of early high-pressure metamorphism (reaching the eclogite facies), as suggested in the previous studies [35].

The results of the conducted studies should be taken into account when determining the belonging of the Kaskama block to one or another Paleoproterozoic terrane of the Kola-Norwegian Region of the Fennoscandian Shield.

The authors thank O.L.Galankina (Institute of Precambrian Geology and Geochronology RAS) for assistance in analytical studies of minerals.

REFERENCES

1. Glaznev V.N. Complex geophysical models of lithosphere of Fennoscandia. Apatity: KaeM, 2003, p. 250.
2. Balagansky V.V., Glaznev V.N., Osipenko L.G. Early Proterozoic evolution of the northeastern Baltic Shield: terrane analysis. *Geotectonics.* 1998. Vol. 32. N 2, p. 81-93.
3. Daly J.S., Balagansky V.V., Timmerman M.J. et al. The Lapland-Kola orogen: Palaeoproterozoic collision and accretion of the northern Fennoscandian lithosphere. *European Lithosphere Dynamics. Geological Society of London*, 2006. Vol. 32, p. 579-598. DOI: 10.1144/GSL.MEM.2006.032.01.35
4. Lahtinen R., Huhma H. A revised geodynamic model for the Lapland-Kola Orogen. *Precambrian Research*. 2019. Vol. 330, p. 1-19. DOI: 10.1016/j.precamres.2019.04.022
5. Vrevsky A.B., Kuznetsov A.B., Lvov P.A. Age and Stratigraphic Position of a Supracrustal Complex (Kaskama Block, Inari Terrane, Northeastern Kola–Norwegian Region of the Fennoscandian Shield). *Doklady Earth Sciences.* 2023. Vol. 511. Part 2, p. 645-651. DOI: 10.1134/S1028334X23600950
6. Daly J.S., Balagansky V.V., Timmerman M.J. et al. Ion microprobe U–Pb zircon geochronology and isotopic evidence for a trans-crustal suture in the Lapland–Kola Orogen, northern Fennoscandian Shield. *Precambrian Research*. 2001. Vol. 105. Iss. 2-4, p. 289-314. DOI: 10.1016/S0301-9268(00)00116-9
7. Pozhilenko V.I., Gavrilenko B.V., Zhirov D.V., Zhabin S.V. Geology of mineral areas of the Murmansk Region. Apatity: Kola Science Centre RAS, 2002, p. 359 (in Russian).
8. Lahtinen R., Salminen P.E., Sayab M. et al. Age and structural constraints on the tectonic evolution of the Paleoproterozoic Saimaa orocline in Fennoscandia. *Precambrian Research*. 2022. Vol. 369. N 106477. DOI: 10.1016/j.precamres.2021.106477
9. Bergman S., Weihed P. Chapter 3: Archean (>2.6 Ga) and Paleoproterozoic (2.5–1.8 Ga), pre- and syn-orogenic magmatism, sedimentation and mineralization in the Norrbotten and Överkalix lithotectonic units, Svecokarelian orogeny. *Sweden: Lithotectonic Framework, Tectonic Evolution and Mineral Resources. Geological Society of London*, 2020. Vol. 50, p. 27-82. DOI: 10.1144/M50-2016-29
10. Lahtinen R., Köykkä J. Multiply deformed Paleoproterozoic foreland fold and thrust belt in northern Fennoscandia – The peripheral Kuusamo belt as a key example. *Precambrian Research*. 2020. Vol. 346. N 105825. DOI: 10.1016/j.precamres.2020.105825
11. Johnston S.T., Lahtinen R., Saumur B.M. et al. Reconstructing the Paleoproterozoic Heart of Nuna, from Fennoscandia to Northeastern Laurentia. *Geological Society, London, Special Publications*. 2024. Vol. 542, p. 31-49. DOI: 10.1144/SP542-2023-37
12. Loucks R.R. A precise olivine-augite Mg-Fe-exchange geothermometer. *Contributions to Mineralogy and Petrology*. 1996. Vol. 125. Iss. 2-3, p. 140-150. DOI: 10.1007/s004100050211
13. MacGregor I.D. Empirical geothermometers and geothermobarometers for spinel peridotite phase assemblages. *International Geology Review*. 2015. Vol. 57. Iss. 15, p. 1940-1974. DOI: 10.1080/00206814.2015.1045307
14. O'Neill H.St.C., Wall V.J. The Olivine–Orthopyroxene–Spinel Oxygen Geobarometer, the Nickel Precipitation Curve, and the Oxygen Fugacity of the Earth's Upper Mantle. *Journal of Petrology*. 1987. Vol. 28, p. 1169-1191. DOI: 10.1093/petrology/28.6.1169
15. Wells P.R.A. Pyroxene Thermometry in Simple and Complex Systems. *Contributions to Mineralogy and Petrology*. 1977. Vol. 62. Iss. 2, p. 129-139. DOI: 10.1007/BF00372872

16. Putirka K. Thermometers and Barometers for Volcanic Systems. *Reviews in Mineralogy and Geochemistry*. 2008. Vol. 69. N 1, p. 61-120. DOI: 10.2138/rmg.2008.69.3

17. Holland T., Blundy J. Non-ideal interactions in calcic amphiboles and their bearing on amphibole-plagioclase thermometry. *Contributions to Mineralogy and Petrology*. 1994. Vol. 116. Iss. 4, p. 433-447. DOI: 10.1007/BF00310910

18. Graham C.M., Powell R. A garnet–hornblende geothermometer: calibration, testing, and application to the Pelona Schist, Southern California. *Journal of Metamorphic Geology*. 1984. Vol. 2. Iss. 1, p. 13-31. DOI: 10.1111/j.1525-1314.1984.tb00282.x

19. Powell R. Regression diagnostics and robust regression in geothermometer/geobarometer calibration: the garnet-clinopyroxene geothermometer revisited. *Journal of Metamorphic Geology*. 1985. Vol. 3. Iss 3, p. 231-243. DOI: 10.1111/j.1525-1314.1985.tb00319.x

20. Perchuk L.L. 5-Derivation of a thermodynamically consistent set of geothermometers and geobarometers for metamorphic and magmatic rocks. Progress in Metamorphic and Magmatic Petrology. Cambridge University Press, 1991, p. 93-112. DOI: 10.1017/CBO9780511564444.007

21. Ravna E.K. Distribution of Fe^{2+} and Mg between coexisting garnet and hornblende in synthetic and natural systems: an empirical calibration of the garnet–hornblende Fe–Mg geothermometer. *Lithos*. 2000. Vol. 53. Iss. 3-4, p. 265-277. DOI: 10.1016/S0024-4937(00)00029-3

22. Holdaway M.J. Application of new experimental and garnet Margules data to the garnet-biotite geothermometer. *American Mineralogist*. 2000. Vol. 85. Iss. 7-8, p. 881-892. DOI: 10.2138/am-2000-0701

23. Mutch E.J.F., Blundy J.D., Tattitch B.C. et al. An experimental study of amphibole stability in low-pressure granitic magmas and a revised Al-in-hornblende geobarometer. *Contributions to Mineralogy and Petrology*. 2016. Vol. 171. Iss. 10. N 85. DOI: 10.1007/s00410-016-1298-9

24. Kohn M.J., Spear F.S. Empirical calibration of geobarometers for the assemblage garnet + plagioclase + quartz. *American Mineralogist*. 1989. Vol. 74. N 1-2, p. 77-84.

25. Kohn M.J., Spear F.S. Two new geobarometers for garnet amphibolites, with applications to southeastern Vermont. *American Mineralogist*. 1990. Vol. 75. N 1-2, p. 89-96.

26. Dale J., Holland T., Powell R. Hornblende–garnet–plagioclase thermobarometry: a natural assemblage calibration of the thermodynamics of hornblende. *Contributions to Mineralogy and Petrology*. 2000. Vol. 140. Iss. 3, p. 353-362. DOI: 10.1007/s004100000187

27. Chun-Ming Wu, Jian Zhang, Liu-Dong Ren. Empirical Garnet–Biotite–Plagioclase–Quartz (GBPQ) Geobarometry in Medium- to High-Grade Metapelites. *Journal of Petrology*. 2004. Vol. 45. Iss. 9, p. 1907-1921. DOI: 10.1093/petrology/egh038

28. Connolly J.A.D. Multivariable Phase Diagrams; an Algorithm Based on Generalized Thermodynamics. *American Journal of Science*. 1990. Vol. 29, p. 666-718. DOI: 10.2475/ajs.290.6.666

29. Holland T.J.B., Powell R. An improved and extended internally consistent thermodynamic dataset for phases of petrological interest, involving a new equation of state for solids. *Journal of Metamorphic Geology*. 2011. Vol. 29. Iss. 3, p. 333-383. DOI: 10.1111/j.1525-1314.2010.00923.x

30. White R.W., Powell R., Holland T.J.B. et al. New mineral activity–composition relations for thermodynamic calculations in metapelitic systems. *Journal of Metamorphic Geology*. 2014. Vol. 32. Iss. 3, p. 261-286. DOI: 10.1111/jmg.12071

31. Green E.C.R., White R.W., Diener J.F.A. et al. Activity–composition relations for the calculation of partial melting equilibria in metabasic rocks. *Journal of Metamorphic Geology*. 2016. Vol. 34. Iss. 9, p. 845-869. DOI: 10.1111/jmg.12211

32. Ariskin A.A., Barmina G.S. COMAGMAT: Development of a Magma Crystallization Model and Its Petrological Applications. *Geochemistry International*. 2004. Vol. 42. Suppl. 1, p. S1-S157.

33. Warr L.N. IMA–CNMNC approved mineral symbols. *Mineralogical Magazine*. 2021. Vol. 85. Iss. 3, p. 291-320. DOI: 10.1180/mgm.2021.43

34. Krivovichev V.G., Gulbin Yu.L. Recommendations for Mineral Formula Calculations from Chemical Analytical Data. *Proceedings of the Russian Mineralogical Society*. 2022. Vol. 151. N 1, p. 114-124 (in Russian). DOI: 10.31857/S0869605522010087

35. Kremenetskii A.A. Metamorphism of the basic Precambrian rocks and genesis of amphibolites. Moscow: Nauka, 1979, p. 112.

36. Hawthorne F.C., Oberti R., Harlow G.E. et al. Nomenclature of the amphibole supergroup. *American Mineralogist*. 2012. Vol. 97. N 11-12, p. 2031-2048. DOI: 10.2138/am.2012.4276

37. Locock A.J. An Excel spreadsheet to classify chemical analyses of amphiboles following the IMA 2012 recommendations. *Computers & Geosciences*. 2014. Vol. 62, p. 1-11. DOI: 10.1016/j.cageo.2013.09.011

38. Petrelli M., Caricchi L., Perugini D. Machine Learning Thermo-Barometry: Application to Clinopyroxene-Bearing Magmas. *Journal of Geophysical Research: Solid Earth*. 2020. Vol. 125. Iss. 9. N e2020JB020130. DOI: 10.1029/2020JB020130

39. Xiaoyan Li, Chao Zhang. Machine Learning Thermobarometry for Biotite-Bearing Magmas. *Journal of Geophysical Research: Solid Earth*. 2022. Vol. 127. Iss. 9. N e2022JB024137. DOI: 10.1029/2022JB024137

40. An-Ping Chen, Hong-Fu Zhang, Ming-Jie Zhang et al. Metamorphic evolution and geological significance of Early Palaeozoic high-pressure granulites from the East Kunlun (NW China). *Journal of Metamorphic Geology*. 2024. Vol. 42. Iss. 4, p. 583-608. DOI: 10.1111/jmg.12767

41. Jorgenson C., Higgins O., Petrelli M. et al. A Machine Learning-Based Approach to Clinopyroxene Thermobarometry: Model Optimization and Distribution for Use in Earth Sciences. *Journal of Geophysical Research: Solid Earth*. 2022. Vol. 127. Iss. 4. N e2021JB022904. DOI: 10.1029/2021JB022904

42. Peacock S. Advances in the thermal and petrologic modeling of subduction zones. *Geosphere*. 2020 Vol. 16. N 4, p. 936-952. DOI: 10.1130/GES02213.1

43. Sakuwaha K.G., Takeshita T., Ahmed A.H. Dataset to evaluate the geology, metamorphic conditions and pseudosection modeling of the Luswishi Dome, Copperbelt, Zambia. *Data in Brief*. 2021. Vol. 39. N 107525. DOI: 10.1016/j.dib.2021.107525

44. Spear F.S., Wolfe O.M., Thomas J.B. et al. P–T Evolution of the Cyclades Blueschist Unit: Constraints on the Evolution of a Nascent Subduction System From Zr-In-Rutile (ZiR) and Quartz-In-Garnet (QuiG) Thermobarometry. *Geochemistry, Geophysics, Geosystems*. 2024. Vol. 25. Iss. 4. N e2023GC011121. DOI: 10.1029/2023GC011121

45. Kaempf J., Johnson T.E., Clark C. et al. Paleoarchean metamorphism in the Acasta Gneiss Complex: Constraints from phase equilibrium modelling and in situ garnet Lu–Hf geochronology. *Journal of Metamorphic Geology*. 2024. Vol. 42. Iss. 3, p. 373-394. DOI: 10.1111/jmg.12759

46. Manzotti P., Regis D., Petts D.C. et al. Formation of multistage garnet grains by fragmentation and overgrowth constrained by microchemical and microstructural mapping. *Journal of Metamorphic Geology*. 2024. Vol. 42. Iss. 4, p. 471-496. DOI: 10.1111/jmg.12761

47. Gulbin Yu.L., Akbarpuran Khaiyati S.A., Sirotkin A.N. Mineral composition and thermobarometry of metamorphic rocks of Western Ny Friesland, Svalbard. *Journal of Mining Institute*. 2023. Vol. 263, p. 657-673.

48. Praharaj P., Rekha S., Bhattacharya A. *P–T* path reconstruction in a multi-layered garnet-bearing schist: Evidence for 2.2–2.1 Ga near-isothermal loading in the northern margin of the Western Dharwar Craton (India), and regional implications. *Geological Journal*. 2024. Vol. 59. Iss. 3, p. 906-933. DOI: 10.1002/gj.4899

49. Abdrakhmanov I.A., Gulbin Yu.L., Skublov S.G., Galankina O.L. Mineralogical Constraints on the Pressure–Temperature Evolution of Granulites in the Bunger Hills, East Antarctica. *Minerals*. 2024. Vol. 14. Iss. 5. N 488. DOI: 10.3390/min14050488

50. Hernández-Uribe D., Holder R.M., Hernández-Montenegro J.D. Eclogite thermobarometry: The consistency between conventional thermobarometry and forward phase-equilibrium modelling. *Journal of Metamorphic Geology*. 2024. Vol. 42. Iss. 1, p. 89-108. DOI: 10.1111/jmg.12747

51. Botao Li, Massonne H.-J., Xiaoping Yuan. A wealth of P–T–t information from metasediments in the HP–UHP terrane of the Pohorje Mountains, Slovenia, elucidates the evolution of the Eastern Alps. *Journal of Metamorphic Geology*. 2023. Vol. 41. Iss. 9, p. 1167-1196. DOI: 10.1111/jmg.12740

52. Baltybaev Sh.K., Yurchenko A.V., Rizvanova N.G. et al. Early Proterozoic Polymigmatites in a Zone of Granulite Metamorphism: *P–T–X* Conditions, Age, and Duration of Migmatization (Northern Ladoga Area, Russia). *Russian Geology and Geophysics*. 2024. Vol. 65. N 7, p. 795-813. DOI: 10.2113/RGG20234600

53. Yurchenko A.V., Baltybaev Sh.K., Volkova Yu.R., Malchushkin E.S. The Mineralogical Composition, Metamorphic Parameters, and Protoliths of Granulites from the Larba Block of the Dzhugdzhur–Stanovoy Fold Area. *Russian Journal of Pacific Geology*. 2024. Vol. 18. N 2, p. 130-149. DOI: 10.1134/S181971402402009X

54. Tiwari A.K., Sarkar T., Karmakar S. et al. Long-lived high-grade metamorphism in southern India: Constraints from charnockites and sapphirine-bearing semipelitic granulites from the Madurai Block. *Journal of Metamorphic Geology*. 2023. Vol. 41. Iss. 9, p. 1261-1297. DOI: 10.1111/jmg.12743

55. Takeshita T., Imayama T., Ando M. et al. Pressure–temperature paths of tectonic blocks in mélange: Recording thermal evolution of a subduction channel at an initial stage of subduction. *Journal of Metamorphic Geology*. 2023. Vol. 41. Iss. 6, p. 787-816. DOI: 10.1111/jmg.12718

56. Yi-Bing Li, Yu-Wen Wu, Bin Su et al. Thermodynamic constraints on the composition of orogenically thickened lower crust. *Journal of Metamorphic Geology*. 2022. Vol. 40. Iss. 8, p. 1405-1426. DOI: 10.1111/jmg.12679

57. Rebay G., Powell R., Holland T.J.B. Calculated phase equilibria for high-pressure serpentinites and compositionally related rocks close to the $MgO–Al_2O_3–SiO_2–H_2O$ (MASH) system. *Journal of Metamorphic Geology*. 2022. Vol. 40. Iss. 7, p. 1219-1234. DOI: 10.1111/jmg.12663

58. Mulligan S.R., Wells M.L., Hoisch T.D. et al. Deviation between quartz-in-garnet elastic geobarometry and equilibrium-based pressure–temperature modelling in Barrovian metamorphic rocks. *Journal of Metamorphic Geology*. 2022. Vol. 40. Iss. 6, p. 1067-1086. DOI: 10.1111/jmg.12658

59. Avedisyan A.A., Balashov Yu.A., Balaganskii V.V. et al. Magmatism, sedimentogenesis and geodynamics of the Pechenga paleoriftogenic structure. Apatity: Kolskii nauchnyi tsentr Rossiiskoi akademii nauk, 1995, p. 164-182.

***Authors*: Aleksandr B. Vrevsky,** *Doctor of Geological and Mineralogical Sciences, Chief Researcher, avrevsky@mail.ru, https://orcid.org/0000-0002-7038-0841 (Institute of Precambrian Geology and Geochronology RAS, Saint Petersburg, Russia; Geological Institute, Kola Science Center of the RAS, Apatity, Russia),* **Anastasiya V. Yurchenko,** *Candidate of Geological and Mineralogical Sciences, Researcher, https://orcid.org/0000-0002-3999-5151 (Institute of Precambrian Geology and Geochronology RAS, Saint Petersburg, Russia),* **Shauket K. Baltybaev,** *Doctor of Geological and Mineralogical Sciences, Chief Researcher, Professor, https://orcid.org/0000-0002-6484-2042 (Institute of Precambrian Geology and Geochronology RAS, Saint Petersburg, Russia; Institute of Earth Sciences, Saint Petersburg State University, Saint Petersburg, Russia).*

The authors declare no conflict of interests.